

Raman spectroscopy of intermolecular charge transfer complex between a conjugated polymer and an organic acceptor molecule

V. V. Bruevich, T. Sh. Makhmutov, and S. G. Elizarov

Faculty of Physics, Lomonosov Moscow State University, Moscow 119992, Russia and International Laser Center, Lomonosov Moscow State University, Moscow 119992, Russia

E. M. Nechvolodova

Semenov Institute of Chemical Physics, Russian Academy of Sciences, Ulitsa Kosygina 4, Moscow 119991, Russia

D. Yu. Paraschuk

Faculty of Physics, Lomonosov Moscow State University, Moscow 119992, Russia and International Laser Center, Lomonosov Moscow State University, Moscow 119992, Russia

(Received 16 March 2007; accepted 6 July 2007; published online 14 September 2007)

Intermolecular donor-acceptor charge transfer complex (CTC) formed in the electronic ground state between poly[2-methoxy-5-(2-ethylhexyloxy)-1,4-phenylenevinylene] (MEH-PPV) and 2,4,7-trinitrofluorenone (TNF) has been investigated by Raman and optical absorption spectroscopies. Blending of MEH-PPV and TNF results in appearance of the CTC absorption band in the optical gap of the both components and in changes in the characteristic MEH-PPV Raman bands including shifts, change in bandwidth, and intensity. The experimental data are similar in films and solutions indicating the CTC formation in both. We associate the low-frequency shift of the strongest MEH-PPV Raman band at $\sim 1580\text{ cm}^{-1}$ reaching 5 cm^{-1} with partial electron transfer from MEH-PPV to TNF amounting $\sim 0.2e^-$. We suggest that polymer conjugated segments can form the CTC of variable composition MEH-PPV:TNF=1:X, where $X \leq 0.5$ is per MEH-PPV monomer unit. Our Raman data indicate that MEH-PPV conjugated segments involved in the CTC become more planar; however, their conjugation length seemingly does not change. © 2007 American Institute of Physics. [DOI: 10.1063/1.2767266]

INTRODUCTION

Conjugated polymers are promising materials for application in various photonic and electronic devices. In recent years much attention has been paid to synthesis of low-band-gap polymers, i.e., with optical gap below 2 eV.¹⁻³ On the other hand, to extend absorption of conjugated polymer materials into the red and near-IR range, one could exploit the properties of donor-acceptor charge transfer complexes (CTCs). As is well known for small π -conjugated molecules, they can easily form donor-acceptor CTCs in the electronic ground state.^{4,5} These CTCs usually have a characteristic absorption band in the optical gap of both the donor and the acceptor. As was shown recently, relatively large π -conjugated molecules such as fullerenes also form CTCs with small molecules such as dimethylaniline,⁶ amines,^{7,8} and a relatively large molecule such as phthalocyanine.⁹ Nonconjugated polymers can form ground-state donor-acceptor CTCs as well, e.g., CTC between polyvinylcarbazole and trinitrofluorenone (TNF) has been thoroughly studied since the 1970s as a photoconductor with sensitivity in the visible spectral range.^{10,11} Intramolecular CTCs of a conjugated polymer have recently been reported for polythiophene,¹² where weak charge transfer occurs within the polymer unit cell including a covalently bound acceptor molecule.

Nevertheless, intermolecular CTCs of conjugated polymers were far less studied. There were reports on CTCs of

oligothiophenes and oligoparaphenylenes with tetracyanoquinodimethane (TCNQ),^{13,14} and Abdou *et al.*¹⁵ reported on a reversible CTC between poly(3-hexylthiophene) and molecular oxygen. We have recently demonstrated that a soluble derivative of poly(paraphenylenevinylene) (MEH-PPV) can form an intermolecular ground-state CTC with low-molecular organic acceptors, specifically with TNF.¹⁶⁻¹⁸ MEH-PPV/TNF blend strongly absorbs in the red and near-IR ranges resulting in generation of mobile charges.¹⁶ These studies suggest that the ground-state CTC is involved in the photophysics, especially energy transfer and charge generation. Moreover, the ground-state CTC influences the donor-acceptor phase separation in the blend¹⁹ and therefore the blend morphology. In turn, the latter has been recognized to be of great importance for the photophysics and charge transport.²⁰ At the same time, blends of conjugated polymers with fullerenes were intensively studied in the last 15 years, and it was generally accepted that charge transfer occurs only in the excited state of the blend but not in its ground state. However, recent studies have shown evidence of a weak ground-state CTC in blends of several conjugated polymers with a soluble derivative of C₆₀, phenyl-C61-butyric-acid-methyl-ester (PCBM).²¹⁻²³ In fact, CTC absorption in polymer/fullerene blends is quite weak, and it was difficult to identify it in the blend absorption spectrum.

Raman spectroscopy is a powerful tool for studying the ground state of π -conjugated chains. It was determined that

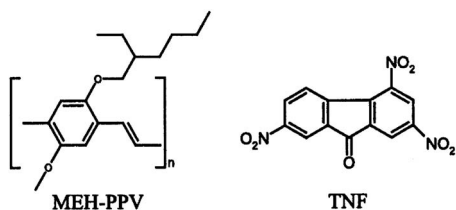


FIG. 1. Chemical structure of MEH-PPV and TNF.

doping corresponding to complete electron transfer from/to the conjugated chain changes essentially its vibrational spectra. In particular, new Raman bands appear upon *p*-doping PPV (Ref. 24) and its oligomers.²⁵ In addition, vibrational spectroscopy of donor-acceptor CTCs of conjugated molecules allows evaluation of the amount of charge transferred in the electronic ground state. For example, typical transferred charge in CTC between tetrathiafulvalene (TTF) and TCNQ is about $0.6e^-$ that was determined from shifts in Raman bands of TTF and TCNQ.²⁶ Raman spectroscopy was also used to identify weak charge transfer ($\sim 0.1e^-$) in fullerene CTCs from 1 to 2 cm^{-1} downshifts of the most intensive C_{60} Raman band at 1470 cm^{-1} .^{8,9}

In this work, extending our previous study,¹⁸ we investigate the ground state of polymer π -conjugated chains forming a donor-acceptor CTC with a low-molecular organic acceptor. Using MEH-PPV as a donor and TNF as an acceptor (Fig. 1), we study changes in optical absorption and Raman spectra of MEH-PPV/TNF blends relative to the spectra of pristine components. We compare these changes in films and solutions and show that the CTC is formed in solution as well as in films. We monitor parameters of the MEH-PPV characteristic Raman bands upon varying TNF content and observe that even at low TNF concentration the majority of Raman active MEH-PPV chains are involved in the CTC. Possible stoichiometry of the MEH-PPV/TNF CTC is discussed. Our Raman data indicate that charge transfer can result in planarization of polymer conjugated segments involved in the CTC. We discuss how CTC could influence their effective conjugation length.

SAMPLES AND EXPERIMENTAL DETAILS

MEH-PPV (Sigma-Aldrich) was dissolved in chlorobenzene at concentration of 2.5–5 g/l for 30–180 min at

60°C . Blends were prepared by mixing chlorobenzene solutions of MEH-PPV and TNF with their molar ratio from 1:0.1 to 1:1 per polymer monomer unit. Films prepared on glass substrates by drop casting and spin casting were used for recording their Raman and optical absorption spectra, respectively.

Absorption spectra were measured in the visible range by using a monochromator MSD-1 (LOMO) equipped with a halogen lamp. The samples were placed right after the exit slit of the monochromator, and the transmitted light was collected by a wide-aperture Si photodetector within a solid angle of $\pi/5$ sr. This was done in order to minimize a contribution of the scattered light to the transmission spectra of MEH-PPV/TNF films.¹⁹ The photodetector signal was processed by using lock-in detection technique. Maximal contribution to the measured optical density of pristine MEH-PPV from its photoluminescence was estimated to be less than 1% of the measured value. The maximum optical density of the spin-cast films was about 0.5.

Raman spectra were recorded using a double monochromator DFS52 (LOMO) equipped by a thermoelectrically cooled photomultiplier (R2949, Hamamatsu). The external cavity diode laser emitting at 670 nm with 2 cm^{-1} full width at half maximum (FWHM) was used as an excitation source.²⁷ To suppress the laser spontaneous emission, combination of a diffraction grating and a slit diaphragm was used. The laser power on the sample was 20 mW. The Raman spectra were measured in the back reflection geometry, normal to the sample surface, in the range of 900–1700 cm^{-1} . They contained a background, which was subtracted after its approximation by a straight line in the range of 150 cm^{-1} around each Raman band.

The FWHM of the spectrometer response function was 6 cm^{-1} . Band frequencies, bandwidths, and intensities were obtained from the measured spectra using the least-squares method. The experimental data within the 15 cm^{-1} bandwidth around the Raman band center were fitted by a Gaussian function in order to minimize influence of possible satellites and background on the result. The approximation error was much less than the experimental random error. Raman bandwidths are presented without correction to the spectrometer response function since we are interested only in their change from one sample to another.

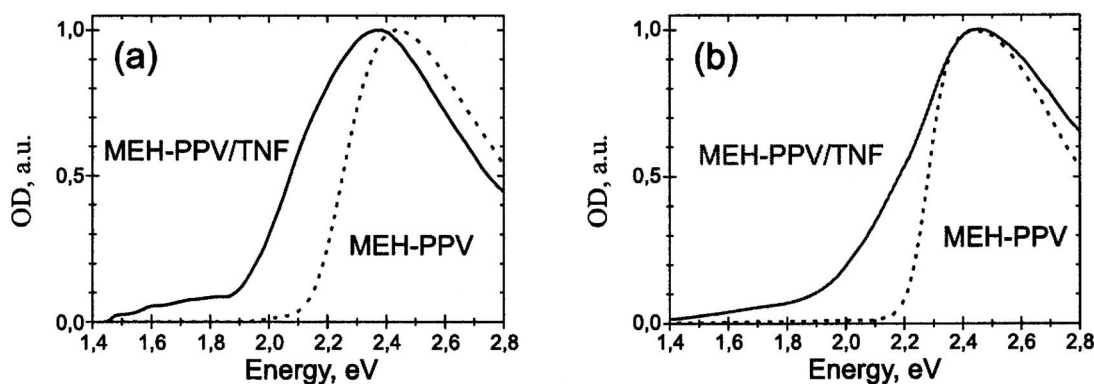


FIG. 2. Absorption spectra of pristine MEH-PPV and MEH-PPV/TNF blend in films (a) and solutions (b). The concentration of MEH-PPV or TNF in solutions was 2.5 g/l.

Since MEH-PPV/TNF blends absorb the Raman scattered radiation differently in the range of 900–1700 cm^{-1} , the Raman band intensities were corrected to the blend absorption spectra. In the one-dimensional backward Raman scattering geometry, the measured $S_m(\lambda)$ and real $S(\lambda)$ Raman spectra are related as follows:

$$S_m(\lambda) \sim \int_0^d S(\lambda) \exp(-x\text{OD}(\lambda_0)/d) \exp(-x\text{OD}(\lambda)/d) dx, \quad (1)$$

where d is the sample thickness, OD is its optical density, λ is the Raman scattering wavelength (varying in the range of 705–760 nm), and λ_0 is the excitation wavelength (670 nm). If the sample is optically thick [$\exp(-\text{OD}) \ll 1$], Eq. (1) gives

$$S(\lambda) \sim S_m(\lambda) [\text{OD}(\lambda_0) + \text{OD}(\lambda)]. \quad (2)$$

Equation (2) was used for correction of the Raman spectra in solutions as they were optically thick. Drop-cast MEH-PPV/TNF films had $\text{OD} \leq 2$ at 670 nm, and we use Eq. (2) to get an upper estimate of the experimental error.

RESULTS

Optical absorption

Figure 2(a) shows absorption spectra of pristine MEH-PPV and MEH-PPV/TNF films. The absorption edge of TNF is about 3.1 eV. Upon addition of TNF, a wide absorption band emerges in the MEH-PPV optical gap. This band was attributed to a donor-acceptor CTC forming between MEH-PPV and TNF.¹⁸ In addition, a redshift of the whole MEH-PPV absorption band is observed, reaching 0.2 eV at its low-frequency edge [Fig. 2(a)]. The intragap absorption and the redshift increased monotonically with TNF concentration saturating at the MEH-PPV:TNF molar ratio of about 1:0.5.¹⁹

Figure 2(b) presents absorption spectra of pristine MEH-PPV and MEH-PPV/TNF blend in chlorobenzene solution. Analogously to the films, the blend in solution shows a long low-frequency tail as compared with the pristine MEH-PPV. However, there is no redshift of the MEH-PPV absorption band in the blended solution [Fig. 2(b)] as compared with the blended film [Fig. 2(a)]. The redshift of MEH-PPV absorption in film might be related to change in polymer effective conjugation length or/and in local dielectric environment of the polymer chains in the blend (see the discussion section below).

Raman scattering

Films

Figure 3 demonstrates Raman spectra of pristine MEH-PPV and equimolar MEH-PPV/TNF blend in films. These spectra are very similar and include seven observed bands of MEH-PPV; their frequencies are shown in Fig. 3. TNF Raman bands are indistinguishable in the spectrum of the blend (lower panel in Fig. 3) as the TNF Raman cross section is much lower than that of MEH-PPV.

The most significant changes in the MEH-PPV Raman spectrum upon TNF addition were observed for two bands peaked approximately at 1580 and 966 cm^{-1} . The strongest

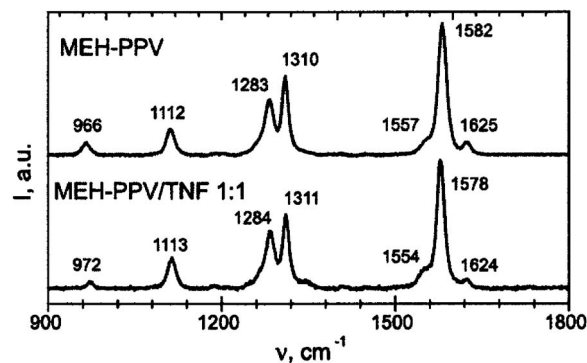


FIG. 3. Raman spectra of pristine MEH-PPV (top) and equimolar MEH-PPV/TNF blend (bottom) in films.

Raman band of 1580 cm^{-1} is assigned to the symmetric stretching vibration of the phenyl ring.^{28,29} The band at 966 cm^{-1} is assigned to the out-of-plane CH bending mode of the vinylene group.^{30,31} This vibration is forbidden in the Raman spectrum for the planar configuration of the polymer chains,³⁰ but it gives a strong band in their IR spectrum.³² However, a weak band at 966 cm^{-1} is observed in Raman spectra of PPV (Refs. 24 and 30) and its soluble derivatives,^{33,34} indicating distortion of the planar conformation of the conjugated polymer chains.

Figure 4(a) presents Raman spectra of MEH-PPV/TNF films in the region of the band of 1580 cm^{-1} for different MEH-PPV:TNF molar ratios. The 1580 cm^{-1} band frequency downshifts with increasing TNF content, with a maximum shift of 3.5 cm^{-1} . At the same time, the narrowing of this band is observed. Low-frequency shift of the 1580 cm^{-1} band in MEH-PPV/TNF films was observed earlier at an excitation wavelength of 1064 nm, and it was attributed to CTC formation between MEH-PPV and TNF in the electronic ground state.¹⁸

As seen in Fig. 4(a), the Raman band at 1557 cm^{-1} observed as a shoulder of the band of 1580 cm^{-1} [Fig. 4(a)] downshifts in the blends as well as the 1580 cm^{-1} band. Similar shifts of the 1557 and 1580 cm^{-1} band frequencies are quite expected since both are assigned mainly to the stretching vibration of the polymer phenyl ring.³¹ As Fig. 4(a) also shows, the band at 1625 cm^{-1} shift noticeably less than the shifts of 1580 and 1557 cm^{-1} bands. The 1625 cm^{-1} band is assigned mainly to the carbon-carbon (CC) stretching vibration of the vinylene group.³¹ At the same time, as one can see in Fig. 4(a), the intensity ratio I_{1557}/I_{1625} monotonically grows with increasing the TNF content (see also Fig. 5). This intensity ratio was suggested to correlate with the conjugation length.^{29,35,36}

Figure 4(b) shows evolution of the MEH-PPV Raman band of 966 cm^{-1} upon addition of TNF. First, the band frequency is upshifted by ≈ 7 cm^{-1} . Second, its intensity is decreased in the blend relative to the other Raman bands (Fig. 3). The intensity ratio I_{960}/I_{1580} drops twice in the blends with the TNF molar ratio $X \geq 0.5$ (MEH-PPV:TNF=1:X) (Fig. 5). Difference in optical absorption of the Raman wavelengths (700–760 nm) appearing in the MEH-PPV/TNF blends (Fig. 2) gives a negligible contribution to decreasing the band of 966 cm^{-1} . Using Eq. (2), we estimate this con-

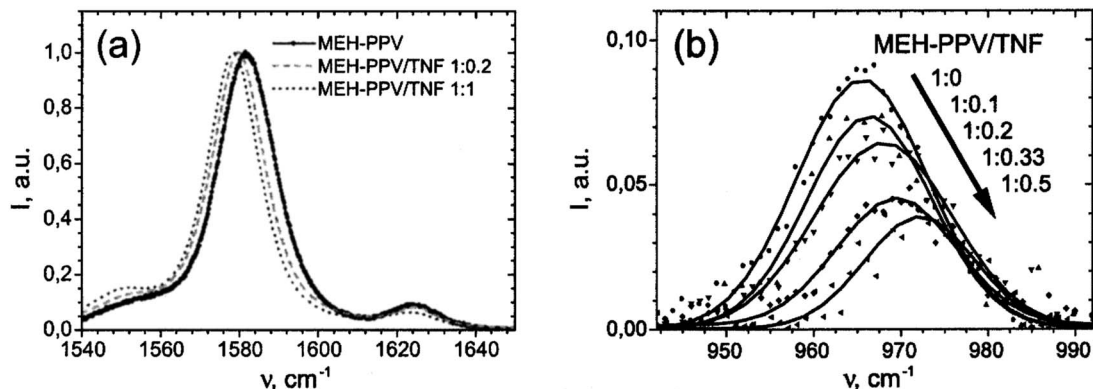


FIG. 4. Raman spectra of MEH-PPV/TNF films normalized to the peak intensity of the 1580 cm^{-1} band for different molar ratios of the components (a) 1580 cm^{-1} and (b) 966 cm^{-1} . The lines in (b) are Gaussian fits.

tribution to be less than 10%. Note that a similar frequency increase of the band of 966 cm^{-1} was also observed in the IR spectra of MEH-PPV/TNF films.³⁷ Simultaneously, the 966 cm^{-1} IR band intensity increased by approximately 50% in the blend with molar ratio of 1:0.4. This behavior of the vibrational mode of 966 cm^{-1} implies better planarity of the polymer chains in the blends and will be discussed below.

Figure 5 summarizes the observed changes in the MEH-PPV Raman spectrum of films as a function of MEH-PPV:TNF ratio. The frequencies of the bands of 966 and 1580 cm^{-1} , the bandwidth of the band of 1580 cm^{-1} , and the intensity ratio I_{966}/I_{1580} are shown. As seen in Fig. 5, these parameters depend monotonically on MEH-PPV:TNF ratio saturating at the ratio of $\approx 1:0.5$.

Solutions

To measure intensity variation of MEH-PPV Raman bands upon addition of TNF in solution, we used the strongest chlorobenzene band at 1003 cm^{-1} as a reference. Indeed, the small amount of MEH-PPV should not affect the Raman spectra of chlorobenzene, and the 1003 cm^{-1} band does not overlap with the MEH-PPV and TNF bands.

Figure 6 displays Raman spectra of MEH-PPV and MEH-PPV/TNF solutions. Similar to the films, the TNF Raman bands are much weaker than the MEH-PPV ones in the blended solution. All the MEH-PPV Raman bands, except the band of 966 cm^{-1} , were a few times stronger in the blend

than in the pristine MEH-PPV. This intensity increase should be assigned to the resonant Raman effect since the excitation wavelength (670 nm) is within the absorption band of the MEH-PPV/TNF blend but beyond that of the pristine MEH-PPV [Fig. 2(a)].

Figure 7 demonstrates Raman spectra of MEH-PPV and MEH-PPV/TNF solutions in the region of the bands of 1580 and 966 cm^{-1} . Similar to the films, addition of TNF results in a frequency downshift of the bands at 1557 and 1585 cm^{-1} (Table I). Note that the downshift of the latter reaches 5 cm^{-1} in solution that is higher than in film. Contrary to the films, the broadening of the band of 1580 cm^{-1} was observed upon addition of TNF (cf. data in Table I and Fig. 5). As in the films, the frequency of band of 966 cm^{-1} is increased and its relative intensity is decreased (Fig. 7). However, the frequency shift ($\sim 3.5\text{ cm}^{-1}$) in solution is approximately two times less than in film, but the relative intensity decreases by a factor of 3 that is noticeably higher than in film. One can suppose that the behavior of the band of 966 cm^{-1} observed both in solution and film is a characteristic feature of CTC formation between MEH-PPV and TNF. Table I summarizes characteristic changes in MEH-PPV Raman spectra upon addition of TNF.

Thus, we observed that the characteristic changes in the Raman and absorption spectra of MEH-PPV/TNF blends upon increasing the TNF content are common in solution and film: appearance of the absorption band in the optical gap of MEH-PPV; frequency downshift of the band of 1580 cm^{-1} ;

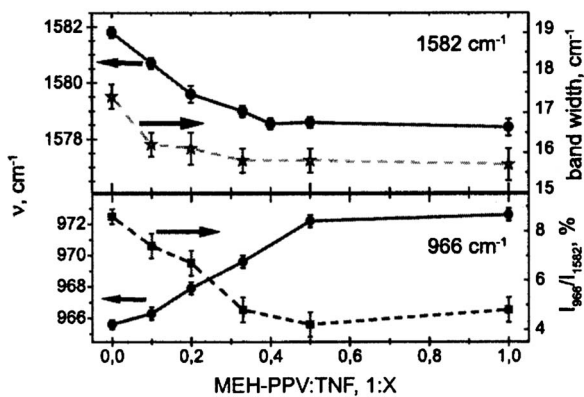


FIG. 5. Parameters of the MEH-PPV Raman bands of 966 and 1580 cm^{-1} in films as a function of TNF molar ratio.

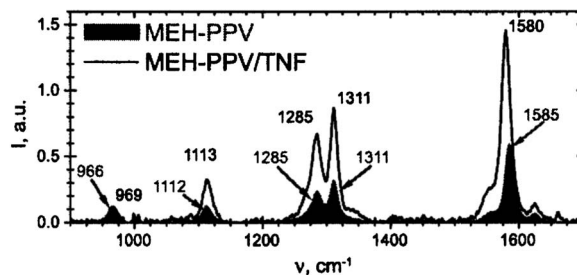


FIG. 6. Raman spectra of MEH-PPV (2.5 g/l) and MEH-PPV/TNF blend (2.5 g/l of MEH-PPV and TNF) in chlorobenzene. Spectra were normalized to the 1003 cm^{-1} chlorobenzene band, and then the chlorobenzene spectrum was subtracted. The MEH-PPV/TNF data were corrected using the absorption spectrum in Fig. 2(b) according to Eq. (2).

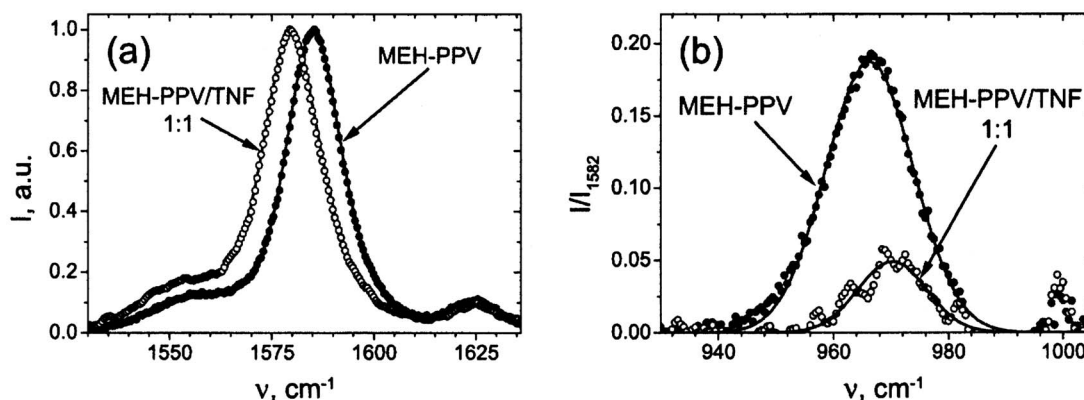


FIG. 7. Raman spectra of MEH-PPV (2.5 g/l) and MEH-PPV/TNF blend (2.5 g/l of MEH-PPV and TNF) solutions of the bands of 1580 cm^{-1} (a) and 966 cm^{-1} (b). Spectra are normalized to the peak intensity of the band of 1580 cm^{-1} . The lines in (b) are Gaussian fits.

intensity decrease of the band of 966 cm^{-1} and its frequency upshift. At the same time, essential difference was observed between the films and solutions: the MEH-PPV absorption band is redshifted only in the films.

DISCUSSION

CTC in solutions and films

MEH-PPV/TNF blends exhibit a new absorption band in the optical gap of both components observed both in solution and film. The intensity of this band normalized to the MEH-PPV main absorption band was nearly the same in both. The strongest Raman MEH-PPV band of 1580 cm^{-1} downshifts in MEH-PPV/TNF blends up to 3.5 cm^{-1} in film and 5 cm^{-1} in solution. These changes in Raman and optical absorption spectra of the blended films were attributed to a donor-acceptor CTC formed in the electronic ground state between MEH-PPV and TNF.^{17,18} Since these changes in the spectra of the blends are very similar in film and solution, one can conclude that the CTC between MEH-PPV and TNF is formed in solution as well.

According to the simplest model of intermolecular CTC by Mulliken,⁵ partial transfer of electron density occurs from the highest occupied molecular orbital (HOMO) of the donor (MEH-PPV) to the lowest unoccupied molecular orbital (LUMO) of the acceptor (TNF) in the electronic ground state. One can expect that decreasing the π -electron density at the bonding HOMO of MEH-PPV results in a downshift of its carbon-carbon stretching vibration frequencies. This explains the observed low-frequency shift of the band of 1580 cm^{-1} . On the other hand, this low-frequency shift might be the result of increase in the conjugation length and/or of variation in the interchain interactions since the

blended films demonstrate also the redshift of the MEH-PPV absorption band [Fig. 2(a)]. Indeed, a redshift of the main absorption band of a conjugated chain is well known to be a characteristic signature of increase in its effective conjugation length. In addition, the interchain interactions can also result in a similar redshift.³⁸ However, we did not observe any redshift of the MEH-PPV absorption band in solution [Fig. 2(b)]. Since the frequency downshift of the Raman band of 1580 cm^{-1} was observed both in film and solution, one can conclude that neither variation in conjugation length nor interchain interaction are the main reason of this shift.

Studies of doped PPV,^{24,25,31,39,40} in which the transferred charge is multiple to the electron charge, have shown that the stretching vibrations of the phenyl ring are quite sensitive to change in π -electron density at the conjugated backbone. Specifically, *p* doping changes the phenyl ring stretching frequencies by about 20 cm^{-1} .^{24,39,40} In low-molecular CTCs,²⁶ the vibrational shifts are shown to be linearly dependent on the amount of the transferred charge. Assuming that this also holds for the MEH-PPV/TNF CTC, one can suggest that the observed downshift of 3.5–5 cm^{-1} of the band of 1580 cm^{-1} corresponds to a decrease in the π -electron density at the polymer conjugated backbone about $0.2e^-$ per monomer unit.

Resonant Raman scattering in CTC

The Raman excitation wavelength of 670 nm corresponds to the CTC absorption band (Fig. 2), implying that the Raman cross section can strongly increase as compared with the pristine MEH-PPV. In fact, the Raman intensities in the blend were about three times higher than in the pristine polymer [Fig. 6(b)] that should be attributed to resonant Raman scattering.

We suggest that the resonant enhancement of Raman intensities in MEH-PPV/TNF film is similar to that in solution. Although absolute Raman intensities were not measured in films, strong resonant Raman enhancement could be observed as a change in the shape and relative intensities of MEH-PPV Raman bands. For example, if just a part of conjugated MEH-PPV chains is involved in the CTC, then only these chains should be observed in Raman spectra as it is usually observed in resonant Raman spectra of conjugated polymers. Nevertheless, our Raman spectra in MEH-PPV/

TABLE I. Parameters of Raman spectra from the data in Fig. 7.

Sample	Frequency (cm^{-1})		FWHM of 1580 (cm^{-1})	I_{966}/I_{1580} (%)
	966 cm^{-1}	1580 cm^{-1}		
MEH-PPV	966.6 \pm 0.3	1584.9 \pm 0.3	15.8 \pm 0.3	18.0 \pm 1.0
MEH-PPV/TNF	970.0 \pm 0.4	1579.8 \pm 0.3	18.7 \pm 0.4	5.6 \pm 1.0

^aCalculated from the peak intensities and corrected using the corresponding absorption spectra according to Eq. (2).

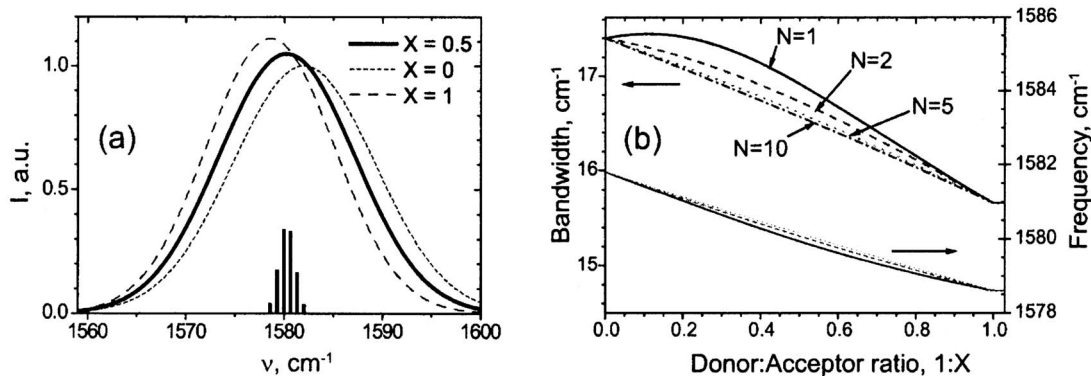


FIG. 8. (a) Calculated Raman spectra of the band of 1580 cm^{-1} for $N=5$ and different X according to Eq. (4), each $F(\nu, \delta_n)$ is a Gaussian function. The bars depict frequencies and intensities of summands in Eq. (4) for $X=0.5$. (b) Bandwidth and frequency of the Raman band of 1580 cm^{-1} as a function of X calculated using Eq. (4) for various N . The data for $X=0$ and 1 are taken from the experiment (Fig. 5).

TNF films at 670 nm excitation are very similar to those measured at 1064 nm excitation¹⁸ despite the fact that the CTC absorption at 1064 nm is at least an order of magnitude less than at 670 nm . Therefore, resonant Raman enhancement at 670 nm should not essentially change the position and the shape of the band of 1580 cm^{-1} .

One can suppose that the observed resonant enhancement in Raman intensity is not very strong because the transition dipole moment vector corresponding to the CTC absorption can be almost perpendicular to the polymer chain direction corresponding to the maximal component of the Raman polarizability tensor. Indeed, intermolecular CTCs of planar conjugated molecules typically have face-to-face configuration of the donor and the acceptor,⁴¹ in which the transition dipole moment corresponding to CTC absorption is nearly perpendicular to both the donor and acceptor planes.^{42,43}

Peculiarities of partial charge transfer from a conjugated chain

The Raman bands of 966 and 1580 cm^{-1} of MEH-PPV shift as a whole upon addition of TNF (Fig. 4). Moreover, the band of 1580 cm^{-1} narrows in films (Fig. 5). Note that the observed monotonic frequency shifts of the MEH-PPV Raman bands qualitatively differ from the behavior of Raman spectra of PPVs upon p or n doping. In fact, variation of the doping level results in redistribution of the Raman intensity between doped and pristine conjugated chains but not in shifts.³⁹

Since both the shape and the frequency of the MEH-PPV Raman bands do not noticeably change in the resonant Raman conditions, shifts of the bands of 966 and 1580 cm^{-1} observed even at low TNF content (Fig. 5) indicate that the most part of Raman active MEH-PPV chains interacts with TNF. Otherwise, asymmetric broadening of the band of 1580 cm^{-1} resulting from superposition of bands corresponding to the CTC and pristine MEH-PPV would be observed, whereas the observed band narrows in film.

One can explain the observed peculiarities of partial charge transfer from polymer conjugated chains observed in the Raman spectra using a simple model. Owing to delocalization of π -electron density along conjugated segments, we

suggest that the charge transfer to an acceptor molecule can occur from the entire segment, and the latter can interact with a number of acceptor molecules. Consider a set of conjugated segments of the same length including N monomer units supposing the following: (i) the overlapping of the acceptor molecular orbitals with the polymer ones, i.e., donor-acceptor contact, is essential only within one monomer unit; (ii) the electronic charge at each monomer unit of the conjugated segment decreases by q/N , where q is the charge transferred from the entire conjugated segment to one acceptor molecule; (iii) all the acceptor molecules form the CTC independently from each other; (iv) the maximum number of acceptor molecules interacting with a conjugated segment is N . As a result, the amount of transferred charge $\delta_n = nq/N$ per monomer unit obeys the binomial probability distribution,

$$P(\delta_n) = C_N^n X^n (1-X)^{N-n}, \quad (3)$$

where C_N^n is the binomial coefficient and X is the acceptor/donor molar ratio corresponding to the probability of the contact between an acceptor molecule and an arbitrary monomer unit. According to our experimental data, the transfer of electron density from MEH-PPV to TNF results in decreasing both the frequency and the bandwidth of the band of 1580 cm^{-1} . Consequently, the Raman spectrum can be presented as a superposition of N bands, with each of these being associated with δ_n ,

$$S(\nu) = \sum_{n=1}^N P(\delta_n) F(\nu, \delta_n), \quad (4)$$

where $F(\nu, \delta_n)$ describes the Raman band shape corresponding to a conjugated segment of length N interacting with n acceptor molecules. We neglect the resonance Raman effect suggesting $\int F(\nu, \delta_n) d\nu = \text{const}$ and assume that both the frequency and the bandwidth of the band of 1580 cm^{-1} depend on δ_n linearly. Figure 8(a) shows Raman spectra of the band of 1580 cm^{-1} calculated from Eq. (4) for $X=0, 0.5, 1$. Note that there is no distribution of Raman frequencies for $X=0$ and 1 in our model as the number of acceptor molecules in the contact with each monomer unit is $0(\delta_0=0)$ and $1(\delta_N=q)$, respectively.

Figure 8(b) demonstrates bandwidths and frequencies of the band of 1580 cm^{-1} calculated from Eq. (4) as a function

of X for different conjugated segment lengths N . As seen in Fig. 8(b), the bandwidth increases for $N=1$ at low acceptor content ($X \leq 0.2$). This is quite evident since the Raman band in this case is a sum of two components corresponding to the complexed and free species with different weights determined by X . However, for longer conjugated segments the bandwidth decreases monotonically with X approaching a straight line for $N \geq 5$ despite the fact that the Raman band for $0 < X < 1$ is a sum of the partial bands of different frequencies. Therefore, the model explains the experimentally observed narrowing of the polymer Raman band observed at low acceptor content (Fig. 5) as a peculiarity of charge transfer from the entire conjugated chain. Note that the data in Fig. 8(b) demonstrate very weak sensitivity to the conjugated chain length for $N > 2$.

Our model predicts the saturation of changes in the Raman spectra with increasing the TNF content at $X=1$, whereas the saturation was experimentally observed at $X \approx 0.5$ (Fig. 5). This discrepancy stems from assumption (i) and can be removed if we suggest that one TNF molecule interacts with two monomer units of MEH-PPV. For example, this can be realized if TNF molecules in the CTC are oriented along the polymer chain since the TNF molecule is longer than the MEH-PPV monomer unit.

We remark that in the blended solution, the band of 1580 cm^{-1} is broadened as compared with the pristine polymer. From our spectroscopic data, we cannot distinguish whether this broadening is associated with superposition of the Raman bands from the CTC and the pristine MEH-PPV or is due to the peculiarities of donor-acceptor charge transfer from the conjugated chains. Because of this we have applied the above model only to films.

Thus, we have considered a simple model explaining the monotonic shift and narrowing of the MEH-PPV Raman band of 1580 cm^{-1} observed upon addition of TNF. The model assumes that an acceptor molecule can accept the electron density from the entire segment, and the latter can donate the electron density to a number of acceptor molecules. Our data suggest that the CTC stoichiometry per MEH-PPV monomer unit could be MEH-PPV:TNF=1: X with $X \leq 0.5$. The minimum X should correspond to the longest conjugated segment in the sample interacting with a single acceptor molecule.

Planarization of MEH-PPV chains in CTC

Both in MEH-PPV/TNF solution and film, the Raman band of 966 cm^{-1} corresponding to the in-phase CH out-of-plane wag of the MEH-PPV vinylene group is noticeably changed (Fig. 5): its intensity is decreased and its frequency is increased upon TNF addition. As mentioned above, this Raman band is indicative of distortion of the polymer conformation from the planar one. As reported in Ref. 30, the higher the frequency of the band at $\sim 970 \text{ cm}^{-1}$ and the lower its Raman intensity, the more planar conformation of PPV conjugated segments is achieved. A typical frequency shift of the vibration mode at $\sim 970 \text{ cm}^{-1}$ associated with planarization of PPV oligomers was $6\text{--}8 \text{ cm}^{-1}$.³⁰ This shift is similar to that observed in the MEH-PPV/TNF blends amounting

3.5 cm^{-1} in solution and 7 cm^{-1} in film. Therefore, the observed behavior of the band of 966 cm^{-1} suggests that the MEH-PPV conjugated segments involved in the CTC become more planar.

If a conjugated chain becomes more planar, one could expect that its conjugation length increases. This conjugation length increase should correspond to a redshift of the polymer absorption band. In the MEH-PPV/TNF blends, such redshift was observed only in film but not in solution (Fig. 2). Therefore, planarization may not lead to increase in the effective conjugation length. Consider possible types of planarization in detail.

Symmetry breaking resulting in appearance of the band of 966 cm^{-1} in Raman spectra of PPV-type polymers can be associated with the following distortion of the planar conformation of the conjugated segments: torsion deformation and bending of their plane. The torsion deformation decreases overlapping of the p electrons and consequently can considerably influence the conjugation length. Accordingly, planarization associated with weakening the torsion deformation should result in increasing the conjugation length of MEH-PPV segments interacting with TNF. Nevertheless, we did not observe any shift in the MEH-PPV absorption in solution that could indicate a change in the conjugation length. On the other hand, one can suppose that the bending deformation of the conjugated chain plane influences overlapping of p orbitals noticeably weaker so that such a deformation might explain planarization of conjugated chains without variation of its effective conjugation length.

Conjugated length of polymer chains involved in CTC

The redshift of the MEH-PPV absorption band in the blend with the CTC was observed only in film but not in solution (Fig. 2). Assume that this redshift is due to increase in the effective conjugation length. This suggestion could be supported by increase in Raman intensity ratio I_{1557}/I_{1625} observed in the MEH-PPV/TNF films [Fig. 4(a)].²⁹ In addition, increase in the effective conjugation length is usually accompanied by a downshift of carbon-carbon stretching vibration frequencies of the conjugated chain.⁴⁴ It is commonly accepted that downshifts of the Raman frequencies and redshift in absorption observed in conjugated polymers upon cooling result mainly from increasing the effective conjugation length.⁴⁵ Our measurements of MEH-PPV Raman and absorption spectra in films upon cooling indicate that a 40 meV redshift in absorption corresponds to the 2 cm^{-1} downshift in the band of 1580 cm^{-1} .⁴⁶ Similar shifts upon cooling were observed in BEH-PPV films,³⁴ which is a symmetrically substituted analog of MEH-PPV.

Therefore, if the 0.2 eV redshift of MEH-PPV absorption edge in the MEH-PPV/TNF film results from increase of the effective conjugation length, then this shift should be accompanied by a frequency downshift of the Raman band of 1580 cm^{-1} by at least a few wave numbers. It is reasonable to expect this shift to be additive to the downshift resulted from charge transfer between MEH-PPV and TNF. Hence, the frequency downshift of the band of 1580 cm^{-1} should be noticeably higher in film than in solution, in which

the effective conjugation length seemingly does not change. However, the maximum observed downshift in film does not exceed 4 cm^{-1} , while it is even higher in solution reaching 5 cm^{-1} . Accordingly, assuming that the transferred charge between MEH-PPV and TNF is nearly the same both in film and solution, one should conclude that increase in the effective conjugation length is not the main reason of the MEH-PPV absorption redshift in film. Note that the latter could still be explained by conjugation length increase if it is accompanied by decrease in the transferred charge between MEH-PPV and TNF. Analysis of this possibility is beyond the scope of the present work.

As the effective conjugation length seemingly does not change upon CTC formation, the redshift in film could be explained by a variation in the local dielectric environment associated with the CTC. For example, as we have suggested above, the polymer chains involved in the CTC become more planar. This planarization could possibly result in more close packing of the chains increasing their polarizability and hence the effective dielectric constant of the film. As a result, the stronger local-field effect in the blended film can induce a redshift as compared with the pristine polymer film.

CONCLUSION

The ground electronic state of MEH-PPV conjugated chains involved in a donor-acceptor CTC with TNF has been studied by Raman and optical absorption spectroscopy in blends in film and solution. We suggest that polymer conjugated segments can form the ground-state donor-acceptor CTC of variable composition MEH-PPV:TNF=1:X, where $X \leq 0.5$ is per MEH-PPV monomer unit, with the maximal electron density transferred from the donor to the acceptor about $0.2e^-$. This charge transfer can result in planarization of the polymer conjugated segments involved in the CTC. Assuming that the amount of transferred charge is nearly the same in film and solution, we conclude that the effective conjugation length of polymer chains involved in the CTC does not noticeably change in spite of their planarization.

Note added in proof. While the paper was under review, other data on CTC absorption between various conjugated polymers/oligomers and organic acceptors molecules in solution were reported by Panda *et al.*⁴⁷

ACKNOWLEDGMENTS

This work was supported in part by European Office of Aerospace Research and Development via the International Science and Technology Center (Project 2666P) and Russian Foundation of Basic Research (No. 07-02-01227a). The authors thank D. S. Martyanov for critical reading of the manuscript.

¹C. Winder, G. Matt, J. C. Hummelen, R. A. J. Janssen, N. S. Sariciftci, and C. J. Brabec, *Thin Solid Films* **403**, 373 (2002).

²B. Lee, V. Seshadri, H. Palko, and G. A. Sotzing, *Adv. Mater. (Weinheim, Ger.)* **17**, 1792 (2005).

³F. L. Zhang, W. Mammo, L. M. Andersson, S. Admassie, M. R. Andersson, L. Inganas, S. Admassie, M. R. Andersson, and O. Ingands, *Adv. Mater. (Weinheim, Ger.)* **18**, 2169 (2006).

⁴R. S. Mulliken, *J. Am. Chem. Soc.* **72**, 600 (1950).

⁵R. S. Mulliken, *J. Am. Chem. Soc.* **74**, 811 (1952).

⁶R. J. Sension, A. Z. Szarka, G. R. Smith, and R. M. Hochstrasser, *Chem. Phys. Lett.* **185**, 179 (1991).

⁷D. K. Palit, H. N. Ghosh, H. Pal, A. V. Sapre, J. P. Mittal, R. Seshadri, and C. N. R. Rao, *Chem. Phys. Lett.* **198**, 113 (1992).

⁸M. Ichida, T. Sohda, and A. Nakamura, *Chem. Phys. Lett.* **310**, 373 (1999).

⁹G. Ruani, C. Fontanini, M. Murgia, and C. Taliani, *J. Chem. Phys.* **116**, 1713 (2002).

¹⁰O. Rocquin and C. Chevrot, *Synth. Met.* **89**, 119 (1997).

¹¹G. Weiser, *J. Appl. Phys.* **43**, 5028 (1972).

¹²P. J. Skabara, I. M. Serebryakov, I. F. Perepichka, N. S. Sariciftci, H. Neugebauer, and A. Cravino, *Macromolecules* **34**, 2232 (2001).

¹³S. Hotta and K. Waragai, *Synth. Met.* **32**, 395 (1989).

¹⁴B. Xu, D. Fichou, G. Horowitz, and F. Garnier, *Synth. Met.* **42**, 2319 (1991).

¹⁵M. S. A. Abdou, F. P. Orfino, Y. Son, and S. Holdcroft, *J. Am. Chem. Soc.* **119**, 4518 (1997).

¹⁶A. A. Bakulin, S. G. Elizarov, A. N. Khodarev *et al.*, *Synth. Met.* **147**, 221 (2004).

¹⁷A. A. Bakulin, A. N. Khodarev, D. S. Martyanov, S. G. Elizarov, I. V. Golovnin, D. Yu. Paraschuk, S. A. Arnautov, and E. M. Nechvolodova, *Dokl. Chem.* **398**, 204 (2004).

¹⁸D. Yu. Paraschuk, S. G. Elizarov, A. N. Khodarev, A. N. Shchegolikhin, S. A. Arnautov, and E. M. Nechvolodova, *JETP Lett.* **81**, 467 (2005).

¹⁹S. G. Elizarov, A. E. Ozimova, D. Yu. Paraschuk, S. A. Arnautov, and E. M. Nechvolodova, *Proc. SPIE* **6257**, 293 (2006).

²⁰H. Hoppe and N. S. Sariciftci, *J. Mater. Chem.* **16**, 45 (2006).

²¹L. Goris, K. Haenen, M. Nesladek, P. Wagner, D. Vanderzande, L. De Schepper, J. D'Haen, L. Lutsen, and J. V. Manca, *J. Mater. Sci.* **40**, 1413 (2005).

²²L. Goris, A. Poruba, L. Hod'akova, M. Vanecek, K. Haenen, M. Nesladek, P. Wagner, D. Vanderzande, L. De Scheper, and J. V. Manca, *Appl. Phys. Lett.* **88**, 052113 (2006).

²³J. J. Benson-Smith, L. Goris, K. Vandewal, K. Haenen, J. V. Manca, D. Vanderzande, D. D. C. Bradley, and J. Nelson, *Adv. Funct. Mater.* **17**, 451 (2007).

²⁴S. Lefrant, E. Perrin, J. P. Buisson, H. Eckhardt, and C. C. Han, *Synth. Met.* **29**, 91 (1989).

²⁵A. Sakamoto, Y. Furukawa, and M. Tasumi, *J. Phys. Chem.* **98**, 4635 (1994).

²⁶R. P. Van Duyne, T. W. Cape, M. R. Suchanski, and A. R. Siedle, *J. Phys. Chem.* **90**, 739 (1986).

²⁷V. V. Bruevich, S. G. Elizarov, and D. Y. Paraschuk, *Quantum Electron.* **36**, 399 (2006).

²⁸F. H. Long, D. McBranch, T. W. Hagler, J. M. Robinson, B. I. Swanson, K. Pakbaz, S. Schricker, A. J. Heeger, and F. Wudl, *Mol. Cryst. Liq. Cryst. Sci. Technol., Sect. A* **256**, 121 (1994).

²⁹E. Mulazzi, A. Ripamonti, J. Wery, B. Dillieu, and S. Lefrant, *Phys. Rev. B* **60**, 16519 (1999).

³⁰A. Sakamoto, Y. Furukawa, and M. Tasumi, *J. Phys. Chem.* **96**, 1490 (1992).

³¹I. Orion, J. P. Buisson, and S. Lefrant, *Phys. Rev. B* **57**, 7050 (1998).

³²D. D. C. Bradley, R. H. Friend, H. Lindemberger, and S. Roth, *Polymer* **27**, 1709 (1986).

³³H. S. Woo, S. C. Graham, D. A. Halliday, D. D. C. Bradley, R. H. Friend, P. L. Burn, and A. B. Holmes, *Phys. Rev. B* **46**, 7379 (1992).

³⁴F. A. C. Oliveira, L. A. Cury, A. Righi, R. L. Moreira, P. S. S. Guimaraes, F. M. Matinaga, M. A. Pimenta, and R. A. Nogueira, *J. Chem. Phys.* **119**, 9777 (2003).

³⁵J. Wery, B. Dillieu, J. Bullo, M. Baitoul, P. Deniard, and J. P. Buisson, *Polymer* **40**, 519 (1999).

³⁶Q. G. Zeng and Z. J. Ding, *J. Phys.: Condens. Matter* **16**, 5171 (2004).

³⁷I. V. Golovnin, E. M. Nechvolodova, and D. Yu. Paraschuk (unpublished).

³⁸B. J. Schwartz, *Annu. Rev. Phys. Chem.* **54**, 141 (2003).

³⁹M. Baitoul, J. Wery, J. P. Buisson, G. Arbuckle, H. Shah, S. Lefrant, and M. Hamdoume, *Polymer* **41**, 6955 (2000).

⁴⁰M. Baitoul, J. Wery, S. Lefrant, E. Faulques, J. P. Buisson, and O. Chauvet, *Phys. Rev. B* **68**, 195203 (2003).

⁴¹M. Saheki, H. Yamada, H. Yoshioka, and K. Nakatsu, *Acta Crystallogr., Sect. B: Struct. Sci.* **32**, 662 (1976).

⁴²S. P. McGlynn, *Chem. Rev. (Washington, D.C.)* **58**, 1113 (1958).

⁴³A. Brillante and M. R. Philpott, *J. Chem. Phys.* **72**, 4019 (1980).

⁴⁴E. Ehrenfreund, Z. Vardeny, O. Brafman, and B. Horovitz, *Phys. Rev. B*

36, 1535 (1987).

⁴⁵J. Yu, M. Hayashi, S. H. Lin, K. K. Liang, J. H. Hsu, W. S. Fann, C.-I. Chao, K. R. Chuang, and S.-A. Chen, *Synth. Met.* **82**, 159 (1996).

⁴⁶M. O. Osotov, V. V. Bruevich, E. M. Nechvolodova, and D. Yu. Parashuk, *International Conference on Coherent and Nonlinear Optics*

(ICONO 2007), 28 May-1 June 2007, Belarus, Technical Digest on CD-ROM, II0-2.

⁴⁷P. Panda, D. Veldman, J. Sweelssen, J. J. A. M. Bastiaansen, B. M. W. Langeveld-Voss, and S. C. J. Meskers, *J. Phys. Chem. B* **111**, 5076 (2007).